FINITE ELEMENT ANALYSIS FOCUSED ON THE FLANGE PLATES AND CONNECTING BOLTS OF RUBER BEARINGS

Mineo TAKAYAMA[1] And Keiko MORITA[2]

SUMMARY

This paper presents the results of finite element analysis of natural rubber bearings with several shape factors including the flange plates and the connecting bolts. This analysis was focused on the distribution of the reaction force and the axial force of the bolts while the rubber bearing was deformed in the horizontal direction. The modelling of the rubber material considering the compressibility was adopted, and this rubber model was applied to this analysis of laminated rubber bearings. From the analysis results, the axial force of bolts and the maximum stress of flange plates do not influenced by the shape of rubber bearing and existence of the central hole. The prediction method of the axial force of the bolt was proposed. Also, the influence of the thickness and property of steel shim plates on the deformation capacity and the stress concentration was discussed briefly.

INTRODUCTION

Authors have carried out the finite element analysis (FEA) to grasp the stress and the strain distributions of laminated rubber bearings[1,2]. Authors mainly examined the reaction force distribution of a laminated rubber bearing and the axial force which works in the mounting bolts from FEA by using the two-dimensional plane strain model[3]. However, in these analyses, the rubber material had been modeled as an incompressible elastomer, and the evaluation of vertical deformation with shearing deformation was insufficient. Then, the modeling of the rubber material considering the compressibility was adopted, and this rubber model was applied to this FEA of laminated rubber bearings. In this paper, the results of FEA carried out using the new rubber material model is described from the viewpoint of bolt axial tension and the maximum stress of the flange plate of rubber bearings. The general-purpose FEA code MARC(K7.2) is used in this analysis.

ANALYTICAL MODEL

Modeling of Rubber Material

Generally, the rubber material is modeled using the strain energy density function *W*. The energy density function used in this analysis is the Eq. (1). This equation was improved in order to consider the compressibility in rubber material model which Ogden proposed.

$$W = \sum_{n=1}^{N} \frac{\mu_n}{\alpha_n} \left[J^{\frac{-\alpha_n}{3}} \left(\lambda_1^{\alpha_n} + \lambda_2^{\alpha_n} + \lambda_3^{\alpha_n} \right) - 3 \right] + 4.5K \left(J^{\frac{1}{3}} - 1 \right)^2 \tag{1}$$

Where, $J = \lambda_1 \lambda_2 \lambda_3$, λ_n is principal stretches, μ_n, α_n are material property, and *K* is bulk modulus. The material property was obtained from simple shear tests of rubber sheets. The rubber material is the natural rubber with shear modulus of 4.5kg/cm^2 (0.45MPa). The size of test pieces of the simple shear test is 25X25mm in planar shape and 6mm in thickness. From the stress-strain relationship obtained by shear testing, the material property was calculated by the least squares method. Table 1 shows the material property used in this analysis.

[1] *Assoc. Prof., Dr.Eng., Faculty of Engineering, Fukuoka University, Email:mineot@fukuoka-u.ac.jp*
[2] *Research Lecturer, Faculty of Engineering, Fukuoka University, Email:keikomt@fukuoka-u.ac.jp*

Table 1 Rubber Material Property used in this Analysis (unit:kg/mm^2)

N	1	2	3	K
μ_n	7.69	3.18×10^{-8}	1.18×10^{-3}	248
α_n	1.22×10^{-2}	2.36	4.84	

Modeling of Steel

The conventional isoparametric four-node plane strain and eight-node brick elements behave poorly in bending. The element (non-conforming element) which corrected the displacement function was used in order to get the good approximation for bending in this analysis. It was confirmed that the bending deformation calculated from the analysis using the non-conforming elements almost perfectly agreed with theoretical prediction. The Young's modulus and Poisson ratio of steel was chosen as 21000kg/mm^2 (206GPa) and 0.3 respectively.

Preliminary Analysis

Figure 1 shows the analytical model for the preliminary analysis. The typical dimensions of the model are 500mm in diameter, 3.75mm in rubber layer thickness, and 26 layers of rubber sheet. The primary shape factor (S_1) of this model is 33.3, and the secondary shape factor (S_2) is 5.1. Three types of the thickness (*ts*) of steel shim plates were used in order to evaluate the effect of steel shims: 3.2mm (1.0*ts*), 2.4mm (0.75*ts*) and 1.6mm (0.5*ts*). Flange plates (25mm thickness, 700mm diameter) were attached in top and bottom of main body of rubber bearing. The analytical mesh was composed of 8 divisions in the circumference and 10 divisions in the radius. Each rubber layer was divided into two parts in the direction of thickness. The steel shim plates (a total of 25 plates) and flange plates were not divided into the direction of thickness. The eight-node isoparametric elements were used. The compressive shearing analysis was carried out with a given compressive load being retained.

Figures 2 shows the restoring force characteristics and the vertical deformation by the analysis as the applied compressive stress (pressure load) is changed from 0 to 500kg/cm^2 (50MPa). The result of the rupture test which carried out under the compressive stress of 150kg/cm^2 is also shown in this figure. The test results and the analytical results show a very good correspondence. Figure 3 shows the change of the restoring force characteristics as bulk modulus K is changed from 0.5 times (0.5K) to double (2.0K). The pressure load is 300kg/cm^2 (30MPa). The vertical deformation is especially largely affected by the change of bulk modulus. Figure 4 shows the restoring force characteristics in modeling steel shim plates as a perfect elasto-plastic material (2400kg/cm^2 yield stress) on the case in which the thickness of steel plate changes. The analytical result using the analytical model with the central hole of 100mmm in diameter is also shown in this figure. The analytical results considering the yielding of steel shims indicate the decrease of the deformation capacity. The vertical deformation increases and the deformation capacity decreases, when the thickness of steel shims is thinner. The existence of the central hole makes the horizontal stiffness small, and the deformation performance deteriorates. Figure 5 shows the relationship between the horizontal stiffness and the compressive stress. The

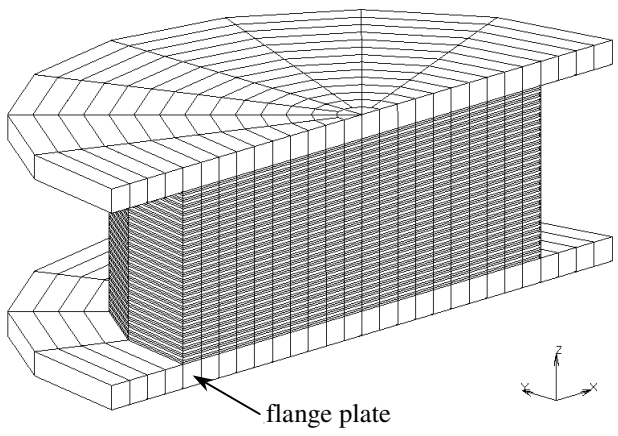

Fig.1 Analytical Model for Preliminary Analysis

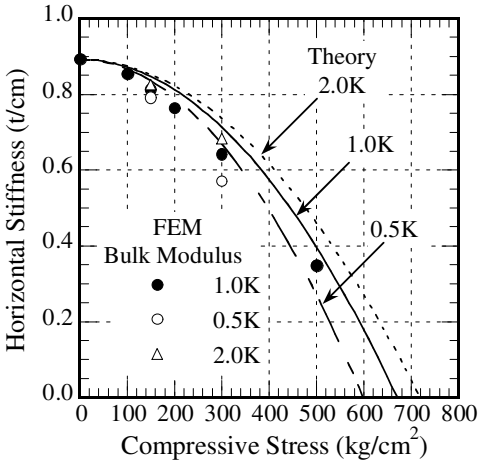

Fig.5 Influence of Axial Load on Stiffness

horizontal stiffness was calculated as the secant rigidity at 100mm in shear deformation. The theoretical relationships are also plotted in the figure. The analytical results and theory show a very good agreement, though the influence of axial load on horizontal stiffness by the analysis is a little bigger than the prediction by theory. The compression stiffness calculated by the FE analysis was almost correspondent to the theoretical values. It was not related either to existence of the central hole and size of the bulk modulus. And, the compression stiffness as the thickness of steel shims changed was completely same. Figure 6 shows the typically deformed shape of the analytical model and the contour of the equivalent stress of steel plates only, when the compressive stress is 300kg/cm^2 and the shear deformation is 300mm. In the case of no central hole, the area of large stress is observed only in the part of upper layers and lower layers of steel shims. The shape of the central hole is transformed in hourglass shape, as the thickness of steel plates is thinner. In the case with central hole, the large stress occurred in the whole steel plates, and almost all shims reached the yield.

ANALYSIS CONSIDERING BOLT AND FLANGE

Analysis Method

The FEA models used in this analysis are shown in Table 2. All analytical models were three-dimensional models with 500mm diameter of rubber layers and 3.5mm thickness of steel shim plates. Two types of thickness of 7mm and 3.5mm were chosen as the rubber layer thickness. The number of rubber layers was decided so that the secondary shape factor (S_2) may become 5 or 3. Total six types of analytical model were used including the model with the central hole of the 100mm diameter. Figure 7 and Figure 8 show the basic dimensions of the analytical model and the modeling of bolts and flange plate. The flange plate (25mm thickness, 800mm diameter) was attached together at top and bottom of rubber bearing main body, and in addition, it was sandwiched between the end plates (t_b=50mm thickness, 900mm diameter) through GAP elements. GAP elements were placed between all nodes of flange plate and base plate. As the characteristics of GAP elements, it rigidly resisted for compression in vertical direction, and it reversibly did not resist for tension. The four bolts at each side was equally placed on the circumference of 350mm in radius (100mm from the edge of rubber bearing). The bolt was modeled in the vertical spring installed between two nodes of the flange plate and the end plate. The stiffness of bolt (vertical spring) was chosen as 1000t/mm. Friction, damping and pre-tension were not consider to GAP elements and springs. The transmission of shearing force between the base plate and the flange plate was modeled by restraining the horizontal displacement between two nodes which the bolt (spring) was connected.

Table 2 Dimensions of Analytical Model

Name	*tr* (mm)	*n*	*Tr* (mm)	S_1	S_2	*ts* (mm)	*d* (mm)	Compressive Stress (kg/cm^2)				
7-14	7.0	14	98	17.9	5.1	3.5	0	0		150	300	
7-24	7.0	24	168	17.9	3.0	3.5	0	0	75	150		
3-28	3.5	28	98	35.7	5.1	3.5	0	0		150	300	450
3-48	3.5	48	168	35.7	3.0	3.5	0	0		150	300	
3-28(100)	3.5	28	98	28.6	5.1	3.5	100	0		150	300	450
3-48(100)	3.5	48	168	28.6	3.0	3.5	100	0		150	300	

tr : Rubber thickness, *n*: Number of rubber layers, *Tr* : Total rubber thickness, *ts* : Steel shims thickness
d : Diameter of central hole, S_1 : Primary shape factor, S_2 : Secondary shape factor

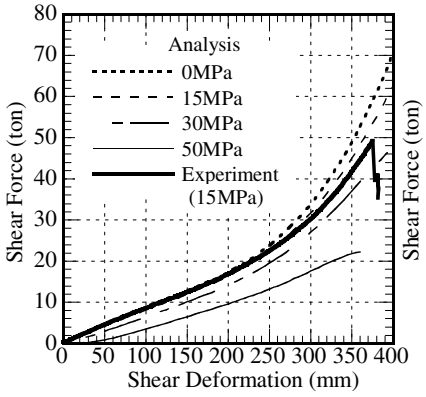

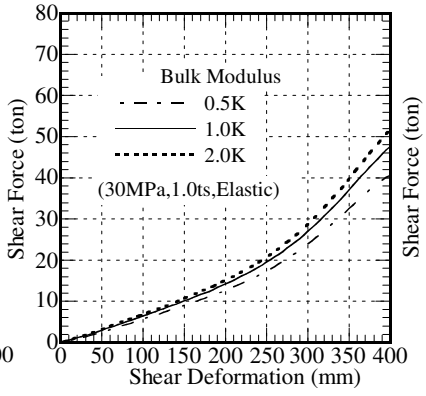

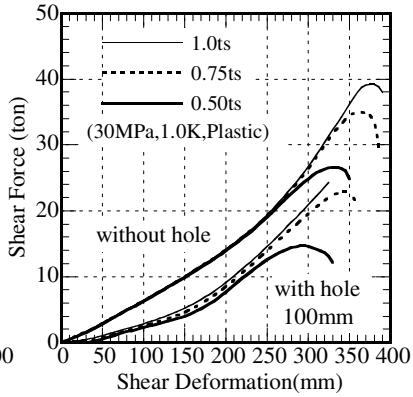

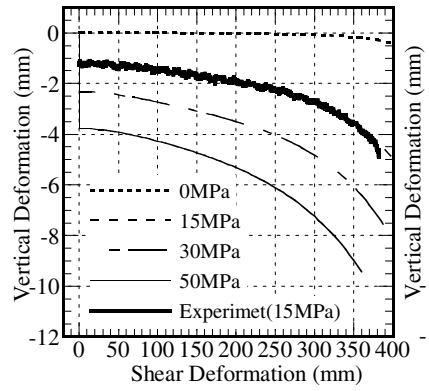

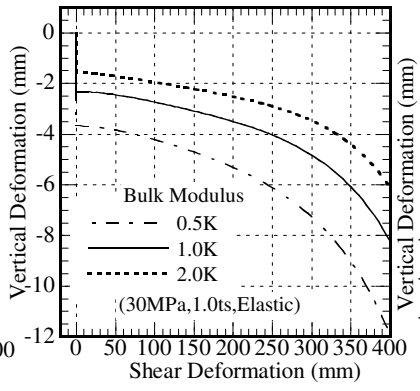

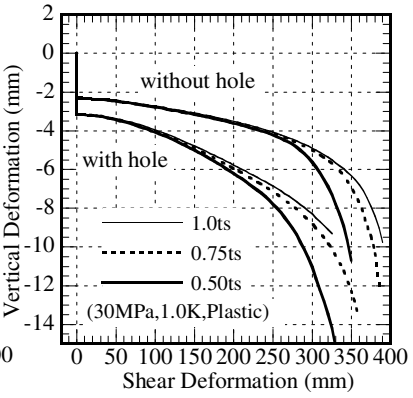

Fig.2 Influence of Axial Stress **Fig.3 Influence of Bulk Modulus** **Fig.4 Influence of Steel Shims**

$$S_1 = \frac{D-d}{4tr},\ S_2 = \frac{D}{Tr} \qquad D : \text{Diameter of steel shims}$$

Figure 9 shows the typical analysis mesh. The mesh representation and the modeling of steel and rubber material were same in the case of the preliminary analysis. The steel plate was modeled as an elastic body. The compressive shearing analysis was carried out. The incremental compressive load (5 ton) was applied up to the pressure shown in Table 2, concentrating on the central node of the uppermost base plate. After that, the same amount of forced horizontal deformation (incremental shear strain is 5%) was applied on all nodes of the uppermost base plate with a given compressive load being retained. The restraining conditions were given so that the displacements in all nodes of the uppermost base plate and the displacement in the node subjected to the concentrated compressive load be identical in the vertical direction. All nodes of the lowermost base plate were restrained in all directions.

Analytical Results

Figure 11 shows the relationship between shear force and shear deformation for all analytical models. Figure 12 shows the eccentricity at GAP elements position (layer). For the restoring force characteristics, the horizontal stiffness decreases, especially in the model with a low secondary shape factor (S_2), as the compressive load is larger. In the model with the central hole, the initial horizontal stiffness indicates a negative value. The eccentricity is almost correspondent with the half of the shear deformation. The effect of the existence of the central hole on the restoring force characteristics and the eccentricity are not observed. Figure 10 shows the forces act to the laminated rubber bearing during shear deformation. From this figure, the balance of the bending moment was shown as follows:

$$M_P + M_Q + M_N = 0 \tag{2}$$

In Eq.(2), M_P, M_Q, M_N was the moment by compressive load, shear force and axial force of bolts respectively. Each moment was obtained as follows:

$$M_P = P_T(\delta - 2e), \qquad M_Q = Q(h - \Delta), \qquad M_N = \sum N_i(l\cos\theta_i - \delta) \tag{3}$$

Where, $P_T = P + N_i$, P: compressive load, δ : shear deformation, e :eccentricity , Q: shear force, h : height of rubber bearing, Δ :vertical deformation, N_i : axial force of bolt, θ_i : angle until bolt position from X-axis, l : bolt interval (P.C.D). Based on the results of 2-D models, the axial force of bolts in one side became the biggest force when the compressive load was 0, but in other side bolts, only little change with just as the value close to 0 was observed. Therefore, the maximum axial force, N_{pre}, of bolts equally placed on the circumference can be estimated by the following equation:

$$N_{pre} \cong \frac{Qh}{l+\delta} \cdot \frac{4}{m} \qquad \text{where, } m\text{: Total number of bolts} \tag{4}$$

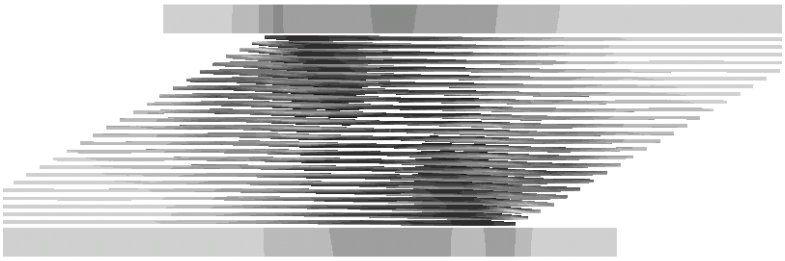

Fig.6(a)
Stress Contour of Steel Plates
(1.0ts, Plastic, without Hole)

Fig.6(b)
Stress Contour of Steel Plates
(1.0ts, Plastic, with Hole)

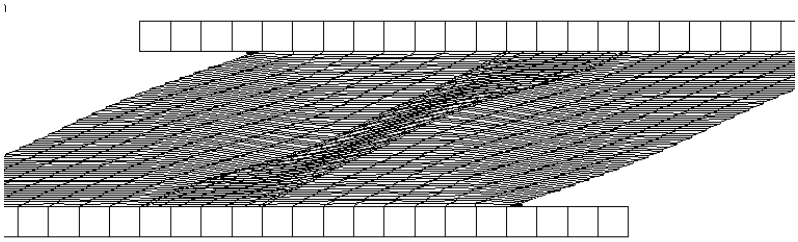

Fig.6(c)
Deformed Shape of Model
(0.5ts, Plastic, with Hole)

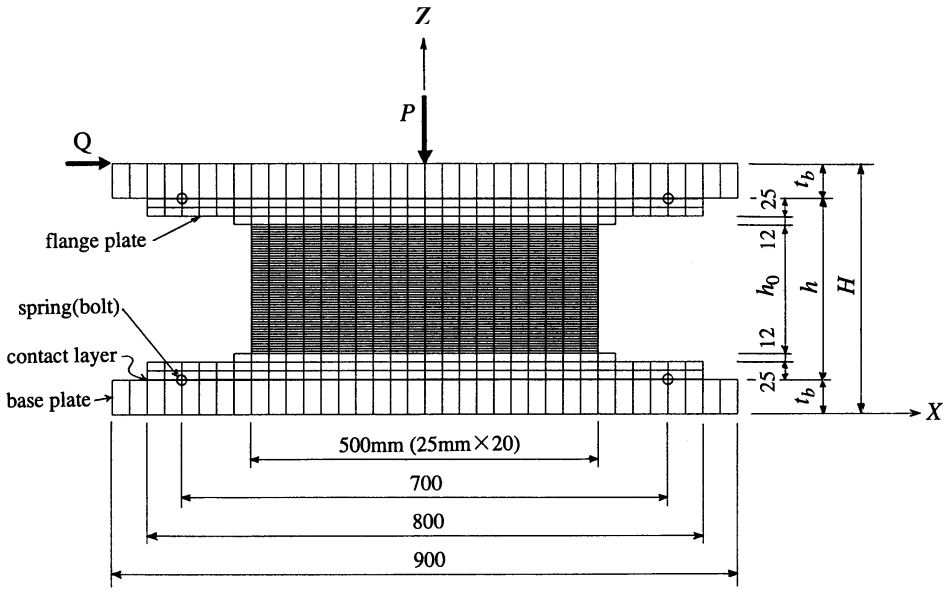

Fig.7 Cross Section of Analytical Model

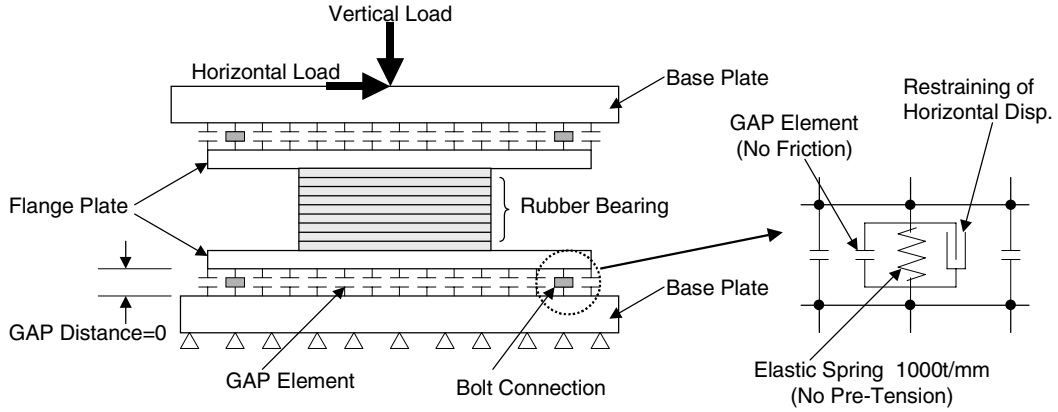

Fig.8 Schematic Diagram for modeling of GAP and Springs

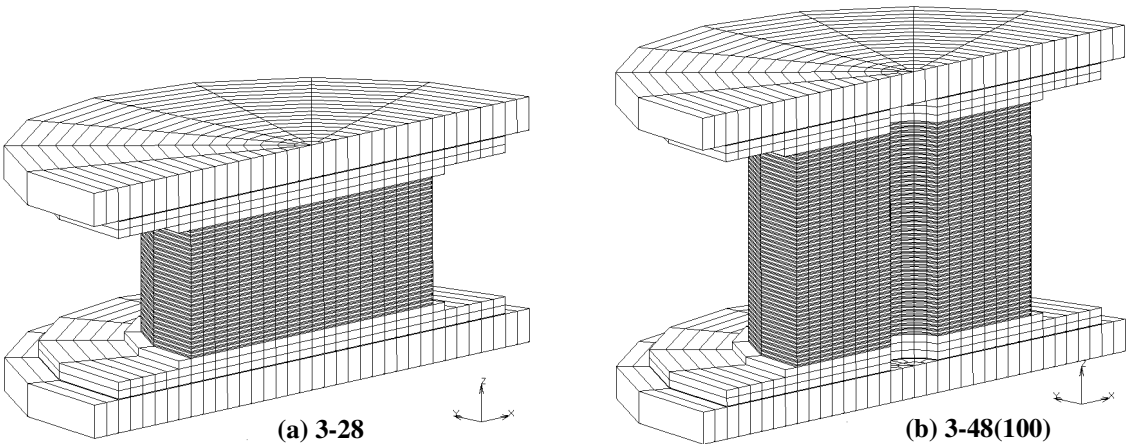

(a) 3-28 **(b) 3-48(100)**

Fig.9 Analytical Models

In the case that the tensile force acts to rubber bearings, the additional axial force of bolts by tensile load is needed to be considered. Figure 13 and Figure 14 show the relationship of the bending moment and the bolt axial tension. In Figure 14, the predicted axial force is also shown by Eq. (4) with the following parameters: the number of bolts m=8, the bolt interval l =70cm. When the compressive load exists, the moment, M_N, by bolt tension is small until about 20cm shear deformation because the additional moment, M_P, by compressive load is balanced against the moment, M_Q, by shear force. The moment by bolt force shows the maximum, when the compressive load is 0. The maximum axial force of bolts occurs without relating to the difference between the analytical models when there is no compressive load as well as the results obtained by the 2-D analysis. The predicted value is almost correspondent to the maximum value of bolt axial tension as there is no compressive load.

Figure 15 shows the maximum equivalent stress (von Mises Stress) of the flange plates by normalizing in the compressive stress. Though all analytical results are shown in the figure, the same tendency is observed without relating to size of the compressive load and shape of the analytical model. The example of the stress contour of the deformed flange plate is also shown. The deformed scale is exaggerated. The maximum stress in the simple compression without shear deformation shows the two times compressive stress as well as estimating by theory. The maximum stress gently increases, as the shearing deformation increases, and the stress rapidly increases from the deformation in which the shear deformation exceed around 25cm. This rapid rise of stress may be caused by the edge effect of laminated rubber bearing. Figure 16 shows the contour of the vertical stress under the 150kg/cm^2 compressive stress. The stress distribution in simple compression loading shows the axial

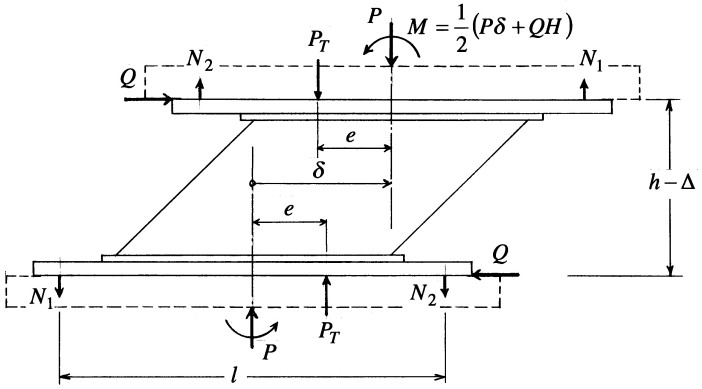

Fig.10 Schematic Diagram of balance of Forces

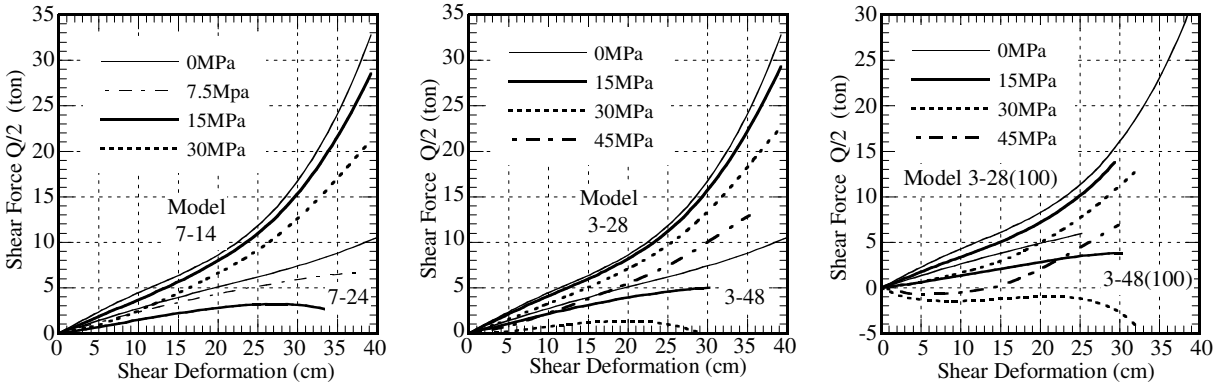

Fig.11 Relationship of Shear Force to Shear Deformation

symmetrical shape, and the maximum stress is about 1.7 times of the compressive stress. The stress in the shearing state is concentrated in overlapped part of upper and lower layer, and the maximum value of vertical stress increases very much.

CONCLUSIONS

The following conclusions can be drawn from this finite element analysis of rubber bearings:

(1) By considering the compressibility of the rubber material, it is possible to more exactly simulate the deformation behavior of laminated rubber bearings.

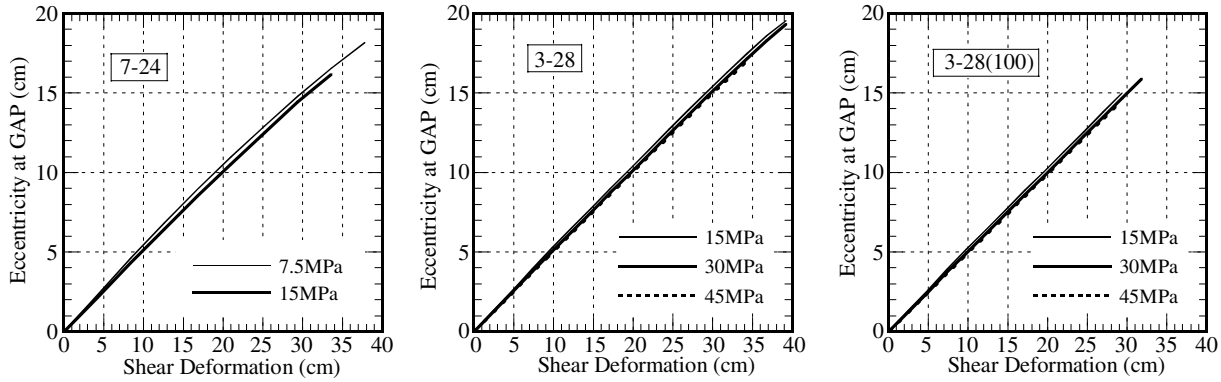

Fig.12 Relationship of Eccentricity at GAP Elements to Shear Deformation

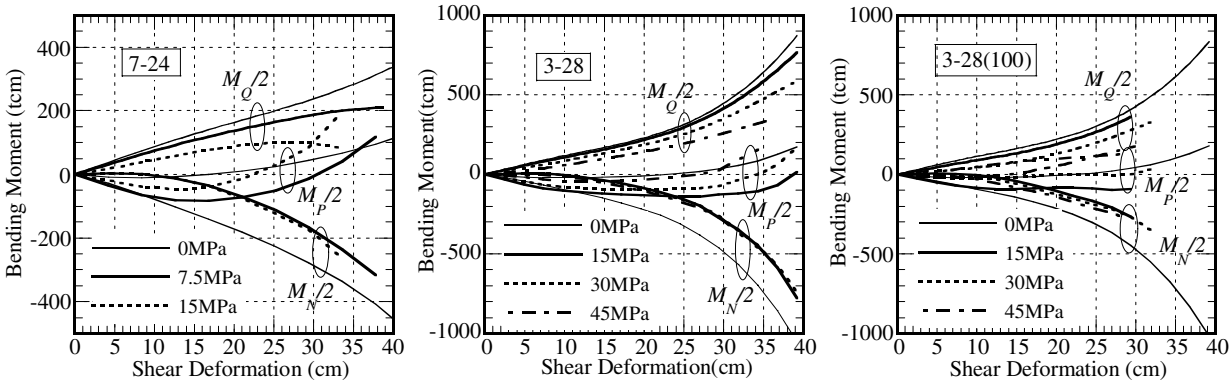

Fig.13 Relationship of Bending Moment to Shear Deformation

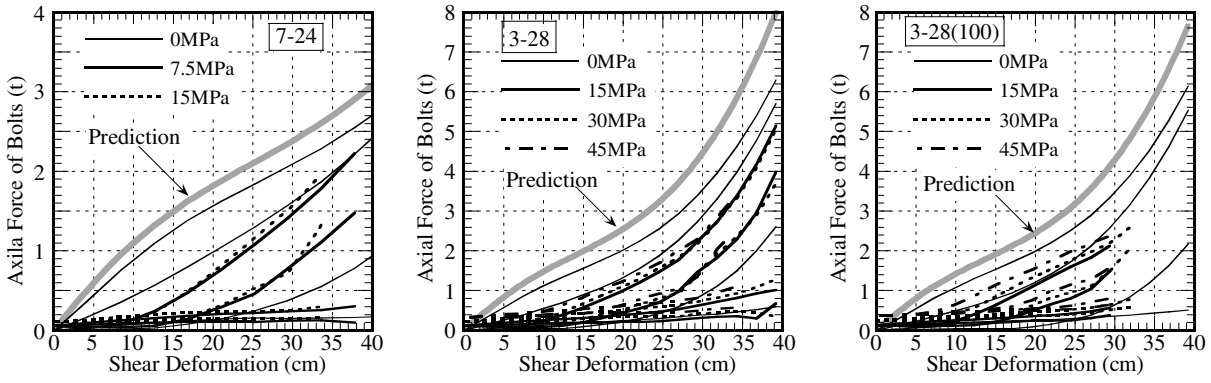

Fig.14 Relationship of Bolt Tension to Shear Deformation

(2) The axial force of bolt and the maximum stress of the flange plate does not effected by the shape of rubber bearing and existence of the central hole, etc.

(3) The eccentricity at the flange plate is almost a half of the shear deformation. It is indicated that the effect of overturning moment by compressive load does not increase in proportion to the shear deformation.

(4) When the compressive load is 0, the axial force of bolt shows the maximum value. The maximum bolt axial tension can be estimated by the equation proposed in this paper.

(5) In the models with central hole, the larger stress occurred in the whole steel shim plates, and the region of plastic part in steel plates expands. When the thickness of steel shims is thinner, the vertical deformation increases and the deformation capacity decreases.

REFERENCES

1) Takayama, M., Tada, H. and Tanaka, R., (1992), "Finite-Element Analysis of Laminated Rubber Bearing used in Base-Isolation System", *Rubber Chemistry and Technology*, Vol.65, No.1, Rubber Division, ACS

2) Takayama, M., Morita, K., (1996), "Maximum Stress of Interlayer Steel Plates in Elastomeric Isolator", PVP-Vol.341, *Seismic, Shock, and Vibration Isolation*, ASME

3) Takayama, M., Morita, K., (1998), "Finite Element Analysis of Rubber Bearings including Flanges and Bolts", PVP-Vol.379, *Seismic, Shock, and Vibration Isolation*, ASME

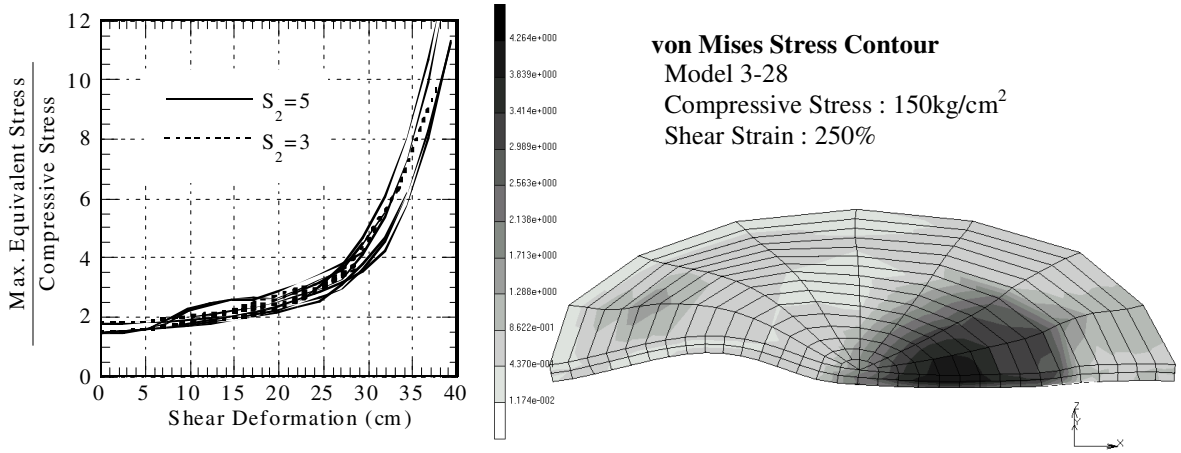

Fig.15 Maximum Equivalent Stress and Typical Deformed Shape of Flange Plate

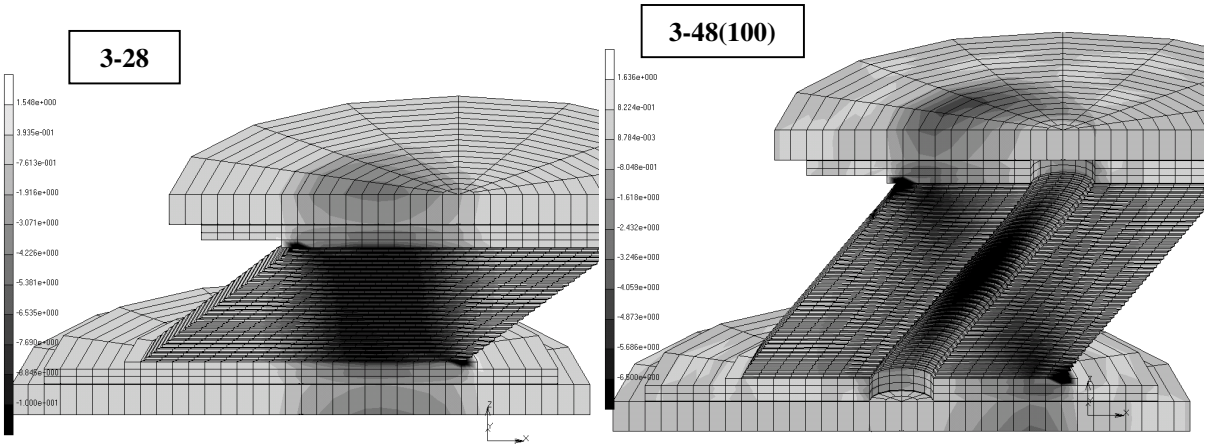

Fig.16 Deformed Shape with Vertical Stress Contour
(Compressive Stress : 150kg/cm^2, Shear Deformation : 25cm)